Characterization of transport properties in gas diffusion layers for proton exchange membrane fuel cells
2. Absolute permeability

Vladimir Gurau [a],[*], Michael J. Bluemle [a], Emory S. De Castro [b], Yu-Min Tsou [b], Thomas A. Zawodzinski Jr. [a], J. Adin Mann Jr. [a]

[a] *Chemical Engineering Department, Case Western Reserve University, 10900 Euclid Avenue, Cleveland, OH 44106-7217, USA*
[b] *E-TEK Division, PEMEAS Fuel Cell Technologies, 41 Veronica Avenue, Somerset, NJ 08873, USA*

Abstract

This is the second in a series of papers in which we present methods demonstrated in our group for the estimation of transport properties in gas diffusion layers (GDLs) for proton exchange membrane fuel cells (PEMFCs). Here we describe a method for determining separately the in-plane (x, y-directions) and through-plane (z-direction), viscous and inertial permeability coefficients of macro-porous substrates and micro-porous layers by controlling the direction of the gas flow through the porous sample. The method is applied initially to the macro-porous substrate of the GDL alone and subsequently to the macro-porous substrate with different micro-porous layers applied on it. The permeability coefficients of the micro-porous layer are calculated from the two measurements. The permeability coefficients are calculated from the Darcy–Forchheimer equation by application of the method of least squares. The method was applied to GDLs having different contents of polytetrafluoroethylene (PTFE) and carbon types. The samples with a higher PTFE content have in-plane and through-plane viscous permeability coefficients higher than those of the samples with lower PTFE content. The in-plane and through-plane viscous permeability coefficients also depend on the carbon type.
© 2007 Elsevier B.V. All rights reserved.

Keywords: Proton exchange membrane fuel cell; Gas diffusion layer; Transport property; In-plane permeability; Through-plane permeability

1. Introduction

The gas diffusion layer (GDL) is a critical contributor to water and reactant management in the proton exchange membrane (PEM) fuel cell. It must simultaneously serve the functions of controlling water transport into and out of the anode and cathode as well as providing high rates of gas transport into the cell. Under the range of operating conditions typical of fuel cells for the automotive environment, the same material must sometimes help to trap water in the membrane in hot and dry environments with low rates of water production (low current) while adapting to high rates of water production at high current, allowing efficient water removal to avoid flooding in the latter case. Furthermore, the GDL must effectively interface with the catalyst coated membrane and flow fields. Because of its central nature, tailoring the GDL provides an opportunity: once we master the details of GDL structure and composition, we will have a powerful and as yet untapped design tool for fuel cells.

To achieve this goal, a wealth of parameters must be understood and controlled. As a starting point we need to be able to assess transport parameters of gas and liquid in-plane and through-plane of the macro-porous and micro-porous layer components.

This paper is the second in a series of papers which cover methods demonstrated in our group for characterization of transport properties in GDLs for PEM fuel cells [1]. Here we develop and elaborate a suite of experimental methods to measure permeability coefficients of the GDL components.

In a PEM fuel cell cathode for each eight units of mass of oxygen consumed per second nine units of mass of water are produced in the electrochemical reaction. In addition, there is water exchange between the ionomer-phase and the pores of the cata-

* Corresponding author. Tel.: +1 216 368 8555; fax: +1 216 368 0953.
  E-mail address: vladimir.gurau@case.edu (V. Gurau).

Nomenclature

a_k	unknown parameters ($k = 1, 2$)
A	vector in Eq. (A.10)
C	matrix in Eq. (A.10)
C_f	flowmeter correction factor
D	diameter of the cylindrical chamber (m)
D_1	inner diameter of the annular GDL sample (m)
D_2	outer diameter the annular GDL sample (m)
f	functional relationship between dependent and independent variables
F	conditional function
k_I	inertial permeability coefficient (m)
k_V	viscous permeability coefficient (m^2)
L	weight factor
μ	dynamic viscosity (N s m^{-2})
M	molecular mass (kg kmol^{-1})
n	number of measurements
n	number of porous layers
P	pressure (N m^{-2})
Q	flow rate (m^3 s^{-1})
ρ	gas density (kg m^{-3})
r	radius (m)
R	residuals
R	universal gas constant (J kmol^{-1} K^{-1})
σ	standard deviation
S	weighted sum of the squares of residuals
T	temperature upstream test fixture (K)
V	gas velocity (m s^{-1}), vector in Eq. (A.10)
w	weights
x	GDL sample thickness (m)
x_j	calculated independent variable ($j = 1, 2, 3$)
X_j	measured independent variable ($j = 1, 2, 3$)
y	calculated dependent variable
Y	measured dependent variable

Subscripts

i	ith layer
tot	total sandwich
0	atmospheric parameters
1	upstream parameters
2	downstream parameters

lyst layer. Supersaturated conditions are commonly encountered at the cathode and thus the water produced is in liquid-phase. Since the gas-phase is consumed in the electrochemical reaction, a negative gas pressure gradient is established from the channels to the catalyst layer. The gas mixture is therefore transported by convection from the cathode flow-field, through the GDL towards the catalyst layer. On the other hand, the liquid water produced must be transported in counter-flow from the catalyst layer, through the GDL into the cathode flow-field. For this to take place, the capillary pressure gradient must overcome the negative pressure gradient of the gas-phase. A high resistance to flow (a low permeability) generates a high gas pressure gradient;

therefore, low GDL permeability coefficients are associated with high liquid water saturation levels in the GDL. This is equivalent to a low GDL effective porosity, which ultimately affects the ability of oxygen to diffuse towards the catalyst layer.

In interdigitated flow-fields gas-phase is forced from high-pressure channels, through the GDL into the adjacent low-pressure channels. In this case the gas-phase is transported through the GDL mainly by convection with in-plane and through-plane velocity components a few orders of magnitude higher than in GDLs adjacent to conventional flow-fields. Both viscous and inertial resistances to flow are responsible for parasitic losses. Thus, information regarding permeability coefficients of the GDL components is of paramount importance in understanding the relationship between GDL chemical and structural properties and its function in the cell.

Absolute GDL permeability coefficients are intrinsic properties depending on the GDL material, but are independent of the gas nature or velocity. The viscous permeability coefficient-k_V (dimensions L^2) reflects the viscous losses between fluid and pore walls. The inertial permeability coefficient-k_I (dimensions L) reflects inertial losses due to changes in the flow direction at the microscopic level (tortuosity) and has been combined with the viscous loss equation of Darcy by Forchheimer (see for example [2]). Since GDL materials are highly anisotropic, the permeability is represented by a rank two tensor. Different permeability coefficients describe the fluid transport 'in plane' (x, y directions), versus 'through plane' (z direction). The 'in-plane' permeability is assumed two-dimensional isotropic and therefore represented by a single coefficient.

Since it is an intrinsic property, the permeability is solely determined by the GDL structure. GDLs are typically multi-layered carbon based porous materials containing a macro-porous substrate or backbone which provides mechanical strength, electrical conductivity and mass transport for the gas reactants and water product, and at least one micro-porous layer which enhances the electrical conductivity and improves the water management. Macro-porous substrates for GDLs can be carbon cloth, carbon fiber papers, or non-woven carbon materials. Since the pore sizes of common macro-porous substrates (1–100 μm) are much larger than the average pore size of catalyst layers (a few hundred nanometers) the electrical contact between the two layers is very poor. The cell performance is considerably improved if a micro-porous layer is attached to the macro-porous substrate in the form of a thin film such as Carbel® (W.L. Gore & Associates, Inc.) or more often, directly integrated into the macro-porous substrate. In the second case, the micro-porous layer consists of a carbon or graphite powder such as an oil-furnace carbon black like Vulcan XC-72R or Black Pearls (Cabot Corp.), an acetylene carbon black like Shawinigan (Chevron Chemical Co.), a graphite like Mogul L or Asbury 850, etc., mixed with a polymeric binder such as polytetrafluoroethylene (PTFE) or polyvinylidene fluoride (PVDF) [3]. The average pore size of the micro-porous layers is comparable to that of catalyst layers. A second advantage of using micro-porous layers is an improved water management.

Macro-porous substrates are highly anisotropic having fibers oriented mainly in-plane (x, y directions). Micro-porous layers are typically isotropic structures. To obtain controlled gradients of GDL properties *E-TEK* Division, PEMEAS Fuel Cell Technologies applies a series of different isotropic micro-porous layers on the macro-porous substrate.

Macro-porous substrates may be impregnated with PTFE to increase the internal contact angle to water and prevent flooding. A typical method of PTFE coating is to immerse the substrate in an aqueous PTFE dispersion such as Hostaflon TF 5032 (Hoechst) or TE 3859 (DuPont) followed by slow solvent evaporation, baking for volatilization of the dispersion agent followed by sintering [4].

The micro-porous slurry is prepared by mechanically mixing the carbon black or graphite powder, with the aqueous PTFE dispersion along with a solvent such as isopropyl alcohol in an ultrasonic bath or magnetic stirrer. Different techniques are used to apply the micro-porous slurry on the macro-porous substrate, including the doctor blade method, screen printing, or spraying. The coating is followed by a slow solvent evaporation, volatilization of the dispersion agent then sintering, similar to the processes described above.

The impact on the porosity and implicitly on the permeability, of the PTFE content in the micro-porous layer is not the same as on the macro-porous substrate. Indeed, Uchida et al. [5] studied the effect of polytetrafluoroethylene (PTFE) content on the porosity of carbon powder (acetylene black)–PTFE systems. The carbon matrix consists of carbon grains (20–40 nm) which form agglomerates of 200–300 nm size. The carbon–PTFE porous structure is therefore characterized by a bi-modal pore size distribution, with primary pores (20–40 nm) inside the agglomerates between the carbon grains and secondary pores (40–200 nm) between the agglomerates. The effect of the PTFE content on the pore-size distribution affects the inter-agglomerate space (secondary pores) but not the intra-agglomerate space (primary pores). The volume of the secondary pores increases with the PTFE (wt.%). The conclusion drawn from these experimental results is that PTFE, due to the molecular size cannot penetrate the intra-agglomerates, but exists in the inter-agglomerate space. It is therefore expected that micro-porous layers which have structures similar to those studied by Uchida will have the porosity and therefore permeability increasing with the PTFE content. On the contrary, when macro-porous substrates are wet-proofed, the PTFE particles partially fill the pores decreasing the porosity and therefore the permeability of the material.

Most of the published papers characterizing GDL permeability report the viscous permeability coefficients in only one direction [6–9]. In other instances, based on the expectation that the inertial resistance to flow in GDLs adjacent to *conventional* flow-fields would be negligible under normal operating fuel cell conditions, researchers lump the viscous and the inertial permeabilities under a single coefficient even when a parabolic dependence of pressure drop on superficial velocity is measured. Some commercially available apparatuses for measuring GDL permeability do not provide capability to interpret such parabolic profiles with two coefficients. Higher-order dissipation term (inertial) may not be neglected a priori. For practical purposes, it may only be neglected when is the case, after it is evaluated. Most probably it may not be neglected for *inter-digitated* applications. There is therefore a need for methods to evaluate simultaneously and at no additional cost both viscous and inertial GDL permeability coefficients.

We present herein a method for determining separately the in-plane (x, y-directions) and through-plane (z-direction), viscous and inertia permeability coefficients of macro-porous substrates and micro-porous layers by controlling rigorously the direction of the gas flow through the porous sample. The method is applied initially to the macro-porous substrate of the GDL alone and subsequently to the macro-porous substrate with different micro-porous layers applied on it. The permeability coefficients of the micro-porous layer are calculated from the two measurements.

Since the viscous and the inertial permeability coefficients are independent of the fluid velocity, we have selected for measurements a range of flow rates such that the accuracy of the experiment is optimal and for which we can clearly distinguish non-linear effects. These velocities are much higher than encounter during normal fuel cell operating conditions in GDLs adjacent to conventional flow-fields, but are within the range of velocities encountered in GDLs adjacent to interdigitated flow-fields. Such an approach, practiced over a range of materials, can tell us which compositions tend toward non-linear behavior and will yield greater insight into the coupling between material properties and transport behavior.

The permeability coefficients are calculated from the Darcy–Forchheimer equation by application of the method of least squares which additionally provides the standard deviation of the estimated parameters. This provides a statistical basis on which to separate the quadratic term (inertial permeability) from the linear term (viscous permeability) rather than lumping both terms in a single coefficient.

Some results obtained using a graphical method have been presented before [10,11].

Determination of relative permeability coefficients for water–gas systems in GDLs will be the subject of a separate paper.

2. Materials and method

Five GDL samples were prepared by *E-TEK* Division, PEMEAS Fuel Cell Technologies (Somerset, New Jersey). Four samples consisted of a single-sided carbon fiber cloth (the macro-porous substrate was the same for all samples) impregnated with a micro-porous sub-layer (four combinations of two different types of carbon and 30 and 70% PTFE loading, respectively) (see also Ref. [1]). A fifth sample consisted of the macro-porous substrate alone (carbon fiber cloth).

The methods used to measure the viscous and inertial permeability coefficients were applied initially to the macro-porous substrate alone and subsequently to the macro-porous substrate with the different micro-porous layers applied on it. The permeability coefficients of the micro-porous layers were calculated from the two measurements.

The experimental set-up for measuring through-plane permeability coefficients is shown in Fig. 1. The GDL sample is clamped between an upstream and a downstream fixture, each
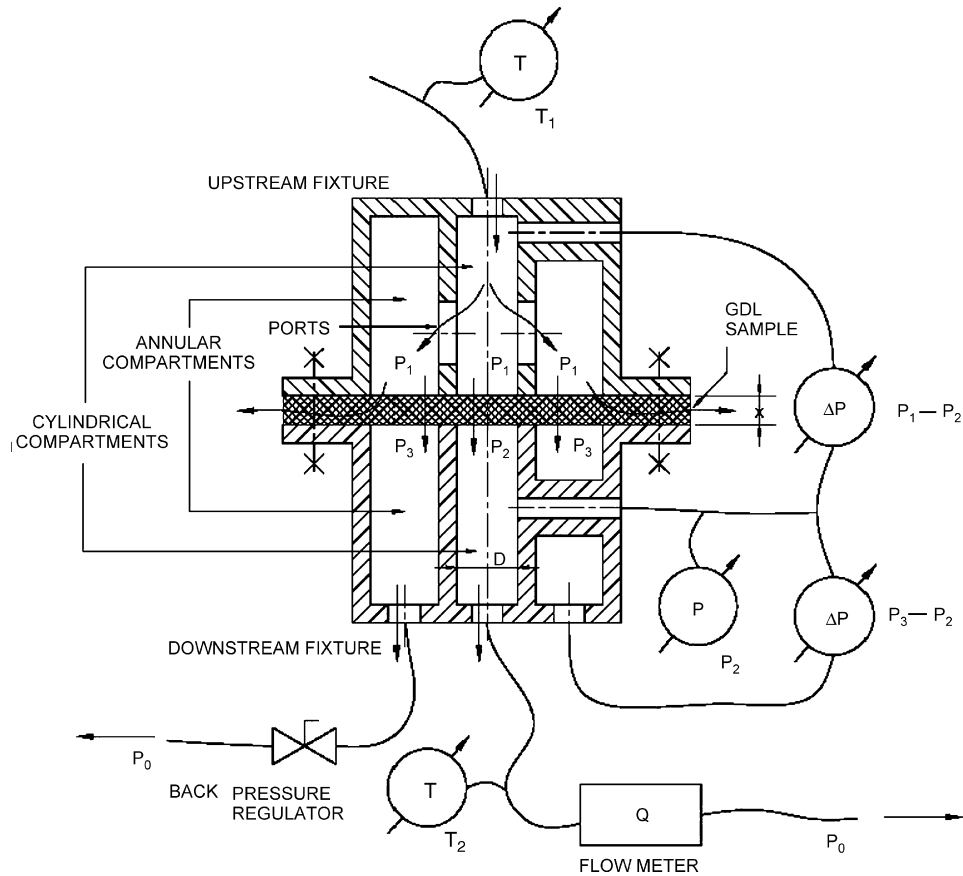
Fig. 1. The experimental set-up for through-plane permeability measurements.

of them consisting of a cylindrical compartment ($D = 1.0$ in.) and an annular compartment. The compartments of the upstream fixture communicate through a number of ports large enough to minimize the pressure drop when gas flows through them. The test gas (dry nitrogen) entering the upstream fixture is divided between the compartments and forced through the GDL sample into the compartments of the downstream fixture. The test gas in the downstream-annular compartment is discharged through a back-pressure regulator into the atmosphere. The flow rate Q through the cylindrical compartments is measured downstream with a rotameter. A pressure-differential gage measures the pressure drop between the upstream-cylindrical compartment and the downstream-cylindrical compartment ($P_1 - P_2$). A second pressure-differential gage measures the pressure difference between the downstream-annular compartment and the downstream-cylindrical compartment ($P_3 - P_2$). An additional pressure gage is used to measure the pressure P_2 in the downstream-cylindrical compartment. The back-pressure regulator is adjusted until pressure P_3 equals pressure P_2 in which case the gas flow through the GDL sample coming from the cylindrical compartment has only a through-plane component (z-direction). Two thermocouples are used to measure the gas temperature upstream, T_1 and downstream, T_2 of the test fixtures. The GDL sample thickness, x is determined from five measurements using a digital micrometer. With the GDL sample set in the fixture, the pressure drop $P_1 - P_2$, the pressure P_2 and the temperatures T_1 and T_2 are measured for approx-

imately twenty different flow rates Q. For each measurement, the back-pressure regulator is adjusted until pressure P_2 equals pressure P_3.

The experimental set-up for measuring in-plane permeability coefficients is shown in Fig. 2a. An annular GDL sample ($D_1 = 1.0$ in., $D_2 = 1.5$ in.) is clamped between an upper and a lower fixture. The gas enters the upper fixture through an inlet opening and is forced through the GDL into the atmosphere in a radial direction (in-plane). This assembly is placed between the platens of a press. The compression force and the sample deformation are measured with a load cell and a strain sensor attached to the upper platen through a support. The initial GDL sample thickness, x was determined from five measurements using a digital micrometer. At different compression levels and for at least five flow rates Q we measured the compression force F, the GDL deformation ΔX, the upstream pressure P_1 and the temperatures T_1 and T_0 upstream and downstream of the test fixture.

The through-plane and in-plane viscous and inertial permeability coefficients were determined from the Darcy–Forchheimer equation by application of the least squares fit analysis method [12]. The least squares method we use assumes Gaussian statistics so that the full maximum likelihood theory is not required. We have included in Appendix A the formulas we use to determine the coefficients, the estimated standard deviations, the correlation coefficients and other measures of goodness of fit.
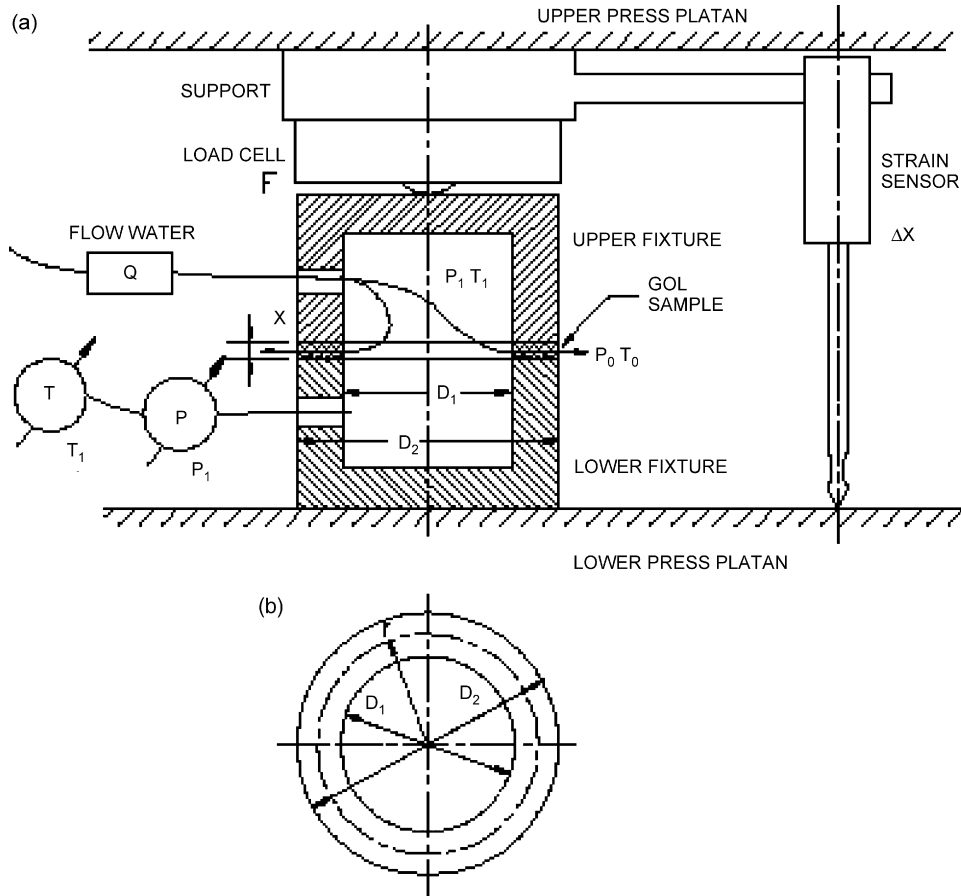
Fig. 2. (a) The experimental set-up for in-plane permeability measurements; (b) the sample for in-plane permeability measurements.

3. Theory and calculation

3.1. Through-plane permeability

We first outline the appropriate analytical approach for the geometry depicted in Fig. 1. The pressure gradient term and the dissipative terms in the momentum transport equation for porous media are orders of magnitude larger than the convective and diffusive terms. Neglecting small terms, the momentum equation reduces to the Darcy–Forchheimer Eq. (1), which describes the relationship between the pressure gradient across the porous sample and the velocity of the fluid flowing through the sample.

$$\frac{\mathrm{d}P}{\mathrm{d}x} = -\frac{\mu}{k_V}V - \frac{\rho}{k_I}V^2 \qquad (1)$$

Since the gas velocity through the porous sample is constant, it is possible to replace the pressure gradient in Eq. (1) with $\Delta P/x$. Note that Eq. (1) naturally provides the requisite second order dependence of pressure drop on superficial velocity. The gas velocity is calculated from the volumetric flow rate through the GDL area located between the cylindrical compartments (Fig. 1):

$$V = \frac{Q}{\pi D^2} \qquad (2)$$

The thermodynamic state of the test gas flowing through the GDL sample is defined by the average temperature and pressure between upstream and downstream ($T = (T_1 + T_2)/2$, $P = (P_1 + P_2)/2$). The gas viscosity μ and density ρ are evaluated at this thermodynamic state.

The mass flow rate of the gas flowing through this area is equal to the mass flow rate through the rotameter at the thermodynamic state defined by T_2 and P_2. Equating the mass flow rates, the expression of the volumetric flow rate through the cylindrical region is:

$$Q = C_f \frac{P_2}{P}\frac{T}{T_2} Q_{\text{indicated}} \qquad (3)$$

where $Q_{\text{indicated}}$ is the volumetric flow rate indicated by the rotameter and C_f is the instrument correction factor, depending on the gas used for calibration and the calibration temperature and pressure.

3.2. Calculation of the through-plane permeability coefficients for the micro-porous layers

When a fluid with viscosity μ and density ρ is forced through a series of porous layers (Fig. 3) with viscous permeability coefficients $k_{V,i}$, inertial permeability coefficients $k_{I,i}$ and thickness
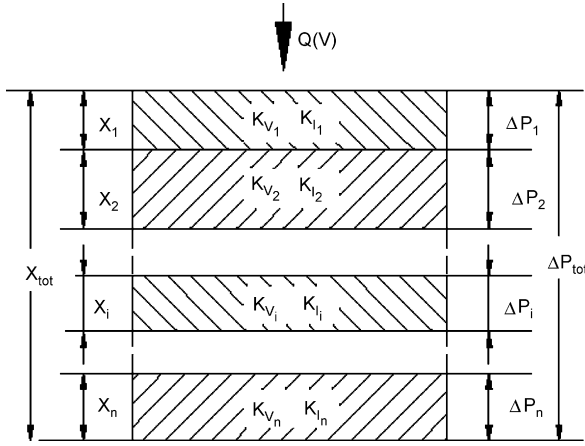
Fig. 3. The model for parallel porous layers.

x_i the total pressure drop experienced by the fluid is:

$$\Delta P_{\text{tot}} = \sum_i \Delta P_i \tag{4}$$

where ΔP_i is the pressure drop through the ith porous layer.

Since the volumetric flow rate (and therefore the fluid velocity) is constant through the sandwich, the Darcy–Forchheimer equation can be written for the entire sandwich and for each individual porous layer in terms of the same velocity V. The Darcy–Forchheimer equation for the entire sandwich is:

$$\frac{\Delta P_{\text{tot}}}{\sum_i x_i} = -\frac{\mu}{k_{\text{V,tot}}} V - \frac{\rho}{k_{\text{I,tot}}} V^2 \tag{5}$$

where $k_{\text{V,tot}}$ and $k_{\text{I,tot}}$ are the equivalent through-plane viscous and inertial permeability coefficients measured for the entire sandwich. For the ith porous layer the Darcy–Forchheimer equation is:

$$\frac{\Delta P_i}{x_i} = -\frac{\mu}{k_{\text{V},i}} V - \frac{\rho}{k_{\text{I},i}} V^2, \quad i = \overline{1, n} \tag{6}$$

using Eqs. (4)–(6) the total pressure drop can be written in terms of the permeability coefficients of the entire sandwich and of each individual layer as:

$$\Delta P_{\text{tot}} = -\mu V \sum_i \left(\frac{x_i}{k_{\text{V},i}} \right) - \rho V^2 \sum_i \left(\frac{x_i}{k_{\text{I},i}} \right)$$

$$= -\mu V \frac{\sum_i x_i}{k_{\text{V,tot}}} - \rho V^2 \frac{\sum_i x_i}{k_{\text{I,tot}}} \tag{7}$$

This identity provides the relationship between $k_{\text{V,tot}}$ and $k_{\text{V},i}$ and $k_{\text{I,tot}}$ and $k_{\text{I},i}$, respectively:

$$k_{\text{V,tot}} = \frac{\sum_i x_i}{\sum_i (x_i / k_{\text{V},i})} \tag{8a}$$

$$k_{\text{I,tot}} = \frac{\sum_i x_i}{\sum_i (x_i / k_{\text{I},i})} \tag{8b}$$

In the particular case when $n = 2$ (GDL consisting of a macro-porous substrate plus a micro-porous layer) and $k_{\text{V},1}$ $k_{\text{I},1}$ (permeability coefficients for the macro-porous substrate) and

$k_{\text{V,tot}}$ and $k_{\text{I,tot}}$ (permeability coefficients for the entire GDL) are known, $k_{\text{V},2}$ and $k_{\text{I},2}$ (permeability coefficients for the micro-porous layer) may be calculated from (8a) and (8b) as:

$$k_{\text{V},2} = \frac{x_2}{(x_{\text{tot}}/k_{\text{V,tot}}) - (x_1/k_{\text{V},1})} \tag{9a}$$

$$k_{\text{I},2} = \frac{x_2}{(x_{\text{tot}}/k_{\text{I,tot}}) - (x_1/k_{\text{I},1})} \tag{9b}$$

3.3. In-plane permeability

For radial flow through the annular sample the Darcy–Forchheimer equation is:

$$\frac{\text{d}P}{\text{d}r} = -\frac{\mu}{k_{\text{V}}} V(r) - \frac{\rho}{k_{\text{I}}} V^2(r) \tag{10}$$

As before, the gas velocity is calculated from the volumetric flow rate:

$$V(r) = \frac{Q}{2\pi r x} \tag{11}$$

where r is the current sample radius (see Fig. 2b).

Since the in-plane dimension of the sample is significantly larger than its thickness, it is important to consider the local gas pressure and density in the derivation of a useful expression for in-plane permeability coefficients. The thermodynamic state of the gas at radius r is therefore defined by the local pressure P and the temperature T; the latter may be considered the average between the upstream and downstream temperatures T_1 and T_0. Equating the mass flow rate of the gas flowing through the cross-sectional area at radius r with the mass flow rate through the rotameter (at the thermodynamic state defined by T_1 and P_1) we find the expression for the local volumetric flow rate:

$$Q = C_{\text{f}} \frac{P_1}{T_1} \frac{T_1 + T_0}{2} \frac{1}{P} Q_{\text{indicated}} \tag{12}$$

After rearranging Eqs. (10)–(12) and integrating one obtains:

$$\frac{P_1^2 - P_0^2}{2} = \frac{A}{k_{\text{V}}} + \frac{B}{k_{\text{I}}} \tag{13a}$$

which is the useful expression for determination of the in-plane permeability coefficients and where

$$A = -\mu C_{\text{f}} \frac{P_1}{T_1} \frac{T_1 + T_0}{2} \frac{Q_{\text{indicated}}}{2\pi x} \ln \frac{D_2}{D_1} \tag{13b}$$

$$B = -2 \left(C_{\text{f}} \frac{P_1}{T_1} \frac{Q_{\text{indicated}}}{2\pi x} \right)^2 \frac{T_1 + T_0}{2} \frac{D_2 - D_1}{D_1 D_2} \tag{13c}$$

4. Results and discussion

4.1. Through-plane permeability

The through-plane viscous and inertial permeability coefficients for the four GDL samples (containing both macro-porous substrate and micro-porous layer) and for the macro-porous substrate alone are presented in Table 1. The margins of error shown

Table 1
Through-plane viscous and inertial permeability coefficients for the entire GDLs and for the macro-porous substrate alone

Sample	$k_V \times 10^{-12}$ (m²)	$k_I \times 10^{-8}$ (m)
Macro-porous substrate and:		
30% PTFE, carbon type 1	0.440 ± 0.005	34 ± 8
70% PTFE, carbon type 1	2.20 ± 0.06	8.0 ± 0.2
30% PTFE, carbon type 2	0.79 ± 0.02	6.3 ± 0.3
70% PTFE, carbon type 2	8.5 ± 0.2	18.6 ± 0.2
Macro-porous substrate alone	13 ± 2	–

in the table represent 95% confidence limit. The results are based on measurements of three or four samples for each batch.

The results show that the samples with a higher PTFE content in the micro-porous layer have viscous permeability coefficients an order of magnitude higher than the corresponding samples with a lower PTFE content. This observation does not contradict the conclusions of Bevers et al. [6] and Park et al. [7] who found that the permeability of carbon fiber paper (macro-porous substrate only) decreases with the PTFE loading. When macro-porous substrates are wet-proofed, for example, by immersion in PTFE dispersion, the PTFE particles will partially fill the pores, decreasing the porosity and therefore the permeability of the material. On the other hand, the PTFE content in the micro-porous layer seems to have a two-fold impact on permeability: first, when the carbon–PTFE mixture is prepared for micro-porous layers, the degree to which the carbon can be dispersed in the mixture depends, among other factors, on the carbon type and the PTFE content. After sintering, the porosity and therefore permeability of the micro-porous layer will depend on the degree of carbon dispersion. As discussed above in this paper, the volume of the secondary pores (macro-pores) between the carbon agglomerates increases with the PTFE content. Second, the PTFE content in the mixture influences the rigidity of the micro-porous layer. We will show below that materials with higher PTFE content are more rigid and therefore maintain higher porosity and in-plane permeability under compressive load.

The results also show that the samples containing carbon type 1 have a lower viscous permeability coefficient than the corresponding samples containing carbon type 2. This probably indicates that carbon type 2 disperses better when mixed with PTFE.

For the range of flow rates controlled with the available rotameter, the resistance to flow through the macro-porous substrate was too low to be detected. Therefore we placed the macro-porous substrate in the fixture in parallel with another porous material for which the permeability coefficients were known. The viscous permeability coefficient of the macro-porous substrate was calculated from Eq. (9a); its higher uncertainty is due to error propagation. The inertial resistance to flow through the macro-porous substrate was found to be negligible.

Fig. 4 shows the plots of pressure gradient vs. the superficial velocity for the four GDLs. Solid lines represent non-linear regression best fit. The general parabolic profiles indicate that both viscous and inertial resistances to flow are significant.
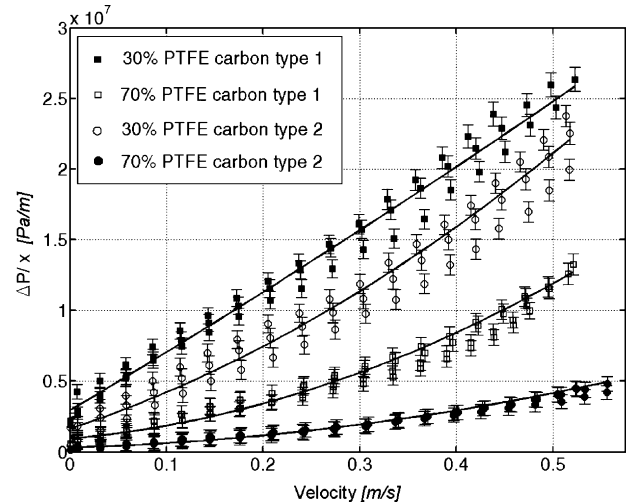

Fig. 4. Pressure gradients vs. through-plane superficial velocity for the entire GDLs. Solid lines represent non-linear regression best fit.

In Table 2 are the through-plane viscous and inertial permeability coefficients for the micro-porous layers calculated with Eqs. (9a) and (9b). Since the inertial resistance through the macro-porous substrate was negligible, the inertial permeability of the GDLs containing macro and micro-porous layers was entirely attributed to the micro-porous layers.

4.2. In-plane permeability

The in-plane viscous permeability coefficient for the entire GDLs and for the macro-porous substrate alone at different compression rates is presented in Table 3 and Fig. 5. The tests showed that the in-plane resistance to flow due to inertia was much lower than the viscous resistance. Therefore the inertial permeability coefficient could not be measured. The margins of error shown in the table represent 95% confidence limit. The results are based on measurements of three or four samples for each batch.

Fig. 6 shows ΔP^2 as a function of in-plane volumetric flow rate, Q for the sample containing 30% PTFE and carbon type 1 at different compression rates. Solid lines represent non-linear regression best fits. Dotted lines represent the bounds of 95% confidence limits. The graphs show a linear variation of ΔP^2 with the in-plane volumetric flow rate indicating that only the viscous resistance to flow is significant for the range of flow rates used in the experiments.

The GDLs containing micro-porous layers with higher PTFE contents have higher in-plane permeability. Materials with carbon type 1 have lower in-plane permeability than materials with

Table 2
The calculated through-plane viscous and inertial permeability coefficients for the micro-porous layers

Sample	$k_V \times 10^{-12}$ (m²)	$k_I \times 10^{-8}$ (m)
30% PTFE, carbon type 1	0.118 ± 0.013	34 ± 8
70% PTFE, carbon type 1	0.64 ± 0.05	8.0 ± 0.2
30% PTFE, carbon type 2	0.09 ± 0.02	6.3 ± 0.3
70% PTFE, carbon type 2	4.9 ± 0.7	18.6 ± 0.2

Table 3
In-plane viscous permeability coefficients for the entire GDLs and for the macro-porous substrate alone

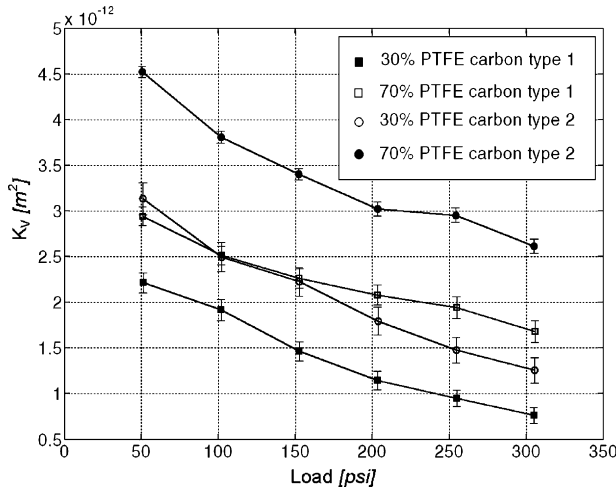| Sample	$k_V \times 10^{-12}$ (m^2)					
	51[a]	102[a]	153[a]	203[a]	255[a]	305[a]
Macro-porous substrate and:						
30% PTFE carbon type 1	2.2 ± 0.1	1.9 ± 0.1	1.4 ± 0.1	1.1 ± 0.1	0.9 ± 0.09	0.7 ± 0.09
70% PTFE carbon type 1	2.9 ± 0.1	2.5 ± 0.1	2.3 ± 0.1	2.1 ± 0.1	1.9 ± 0.1	1.7 ± 0.1
30% PTFE carbon type 2	3.1 ± 0.2	2.5 ± 0.2	2.2 ± 0.2	1.8 ± 0.2	1.5 ± 0.1	1.3 ± 0.1
70% PTFE carbon type 2	4.5 ± 0.06	3.8 ± 0.06	3.4 ± 0.06	3.0 ± 0.08	3.0 ± 0.08	2.6 ± 0.08
Macro-porous substrate alone	17.4 ± 0.2	12.1 ± 0.3	10.8 ± 0.4	10.2 ± 0.5	10.0 ± 0.6	10.1 ± 0.6

[a] Load (psi).

Fig. 5. The in-plane viscous permeability coefficients as a function of compression load for the entire GDLs.

carbon type 2. The same trends were observed for through-plane permeability and we have attributed these findings to the impact the PTFE loading has on the inter-agglomerate porosity (macro-pores) of the micro-porous layer. The PTFE content also influences the GDL rigidity and therefore its capability to
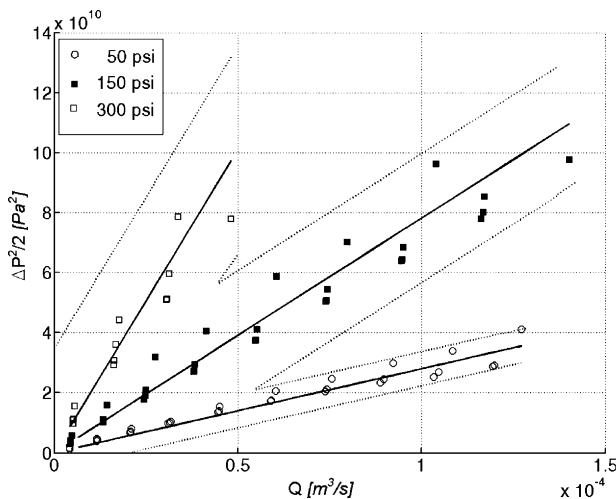

Fig. 6. ΔP^2 as a function of in-plane volumetric flow rate for the sample containing 30% PTFE and carbon type 1 and different compression rates. Solid lines represent non-linear regression best fit. Dotted lines represent the bounds of 95% confidence limit.
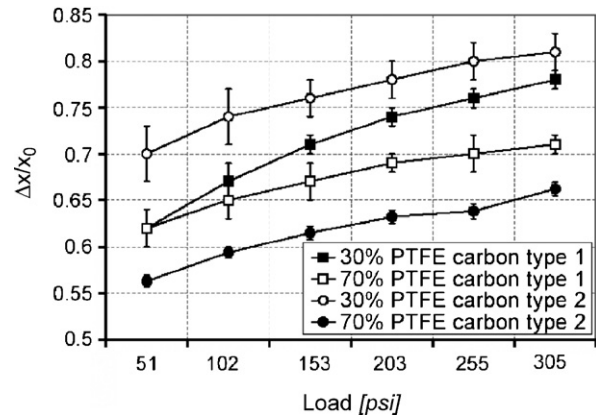

Fig. 7. The strain–stress curves for the entire GDLs.

maintain higher porosity and permeability under compressive load. Fig. 7 presents the strain–stress curves obtained for the four GDLs. Indeed, the samples containing micro-porous layers with 70% PTFE are the samples with the lowest relative deformation.

The in-plane permeability coefficients of the micro-porous layers cannot be calculated from the values for the entire GDLs and for the macro-porous substrate using expressions similar to (9a) and (9b). However, since the micro-porous layers are amorphous mixtures of carbon and PTFE, the in-plane permeability coefficients are expected to be equal to the through-plane coefficients determined before.

5. Conclusions

In this paper we present methods for determining through-plane and in-plane, viscous and inertial permeability coefficients of macro-porous substrates and micro-porous layers of gas diffusion layers for proton exchange membrane fuel cells. The permeability coefficients are determined by strictly controlling the direction of flow through the GDL sample.

The permeability coefficients are measured initially for the entire GDL containing macro-porous substrate and micro-porous layer, and for the macro-porous substrate alone. The permeability coefficients for the micro-porous layer are calculated from these results.

The methods were applied for GDL samples having the same macro-porous substrate and different micro-porous layers (four

combinations of two carbon types and two PTFE loadings). The GDLs having micro-porous layers with the higher PTFE content have higher permeability coefficients. The impact of PTFE content on permeability is two-fold. First, the PTFE loading increases the volume of the intra-agglomerate pores, which further influences the permeability after sintering. Second, the PTFE loading increases the material rigidity, increasing its capability to maintain higher porosity and permeability under compressive load.

The GDLs with micro-porous layers consisting of carbon type 1 have lower permeability than the GDLs containing carbon type 2. This finding was attributed to a better capability of carbon type 2 to be dispersed in the mixture and provide higher porosity and permeability after sintering.

Acknowledgements

Appendix A

A.1. Method of least squares

The through-plane and in-plane viscous and inertial permeability coefficients have been determined using the method of least squares [12], which provides in addition the standard deviation of the estimated parameters.

The physical laws (1) and (13a) are rewritten as:

$$y = a_1 x_1 x_2 + a_2 x_1^2 x_3 \tag{A.1}$$

or as a functional relationship between the dependent and independent variables:

$$y = f(a_1, a_2, x_1, x_2, x_3) \tag{A.2}$$

For through-plane flow the dependent variable is $y = \Delta P/x$, the independent variables are $x_1 = V$, $x_2 = -\mu$, $x_3 = -\rho$ and the unknown parameters are $a_1 = 1/k_v$ and $a_2 = 1/k_I$. For in-plane flow the dependent variable is $y = (P_1^2 - P_0^2)/2$, the independent variables are, $x_1 = Q_{\text{indicated}}$, $x_2 = \mu C_f(P_1/T_1)((T_1 + T_0/2)(1/2\pi x) \ln(D_2/D_1)$, $x_3 = -2(C_f(P_1/T_1)(1/2\pi x))^2((T_1 + T_0/2)((D_2 - D_1)/D_1 D_2)$ and the unknown parameters are $a_1 = 1/k_v$ and $a_2 = 1/k_I$.

The residuals are defined as the difference between the measured and calculated values of the dependent and independent variables, respectively:

$$R_{y_i} = Y_i - y_i, \quad R_{x_{j,i}} = X_{j,i} - x_{j,i}, \quad j = 1, 2, 3 \tag{A.3}$$

The weights are defined as the reciprocal of the squares of the measurement uncertainties (standard deviations):

$$w_{y_i} = \frac{1}{\sigma_{y_i}^2}, \quad w_{x_{j,i}} = \frac{1}{\sigma_{x_{j,i}}^2} \tag{A.4}$$

The method of least squares consists in determining the values of parameters a_1 and a_2 which minimize the weighted sum of the squares of residuals:

$$S = \sum_{i=1}^{n} \left(w_{y_i} R_{y_i}^2 + \sum_{j=1}^{3} w_{x_{j,i}} R_{x_{j,i}}^2 \right) \tag{A.5}$$

The conditional function is defined as:

$$F^i = y_i - f(a_1, a_2, x_1, x_2, x_3) \tag{A.6}$$

The initial guess of the unknown parameters is a_1^o and a_2^0. The initial value of the conditional function is estimated from measurements and the initial guess of the unknown parameters:

$$F_0^i = Y_i - f(a_1^0, a_2^0, X_1, X_2, X_3) \tag{A.7}$$

The weight factor for each measurement is defined as:

$$L_i = \frac{1}{w_{y_i}} \left(\frac{\partial F^i}{\partial y} \right)^2 + \sum_{j=1}^{2} \frac{1}{w_{x_{j,i}}} \left(\frac{\partial F^i}{\partial x_{j,i}} \right) \tag{A.8}$$

The optimized values of the unknown parameters are calculated as:

$$A = C^{-1} V \tag{A.9}$$

where

$$A = \begin{bmatrix} a_1^0 - a_1 \\ a_2^0 - a_2 \end{bmatrix},$$

$$C = \begin{bmatrix} \sum_{i=1}^{n} \frac{1}{L_i} \frac{\partial F^i}{\partial a_1} \frac{\partial F^i}{\partial a_1} & \sum_{i=1}^{n} \frac{1}{L_i} \frac{\partial F^i}{\partial a_1} \frac{\partial F^i}{\partial a_2} \\ \sum_{i=1}^{n} \frac{1}{L_i} \frac{\partial F^i}{\partial a_1} \frac{\partial F^i}{\partial a_2} & \sum_{i=1}^{n} \frac{1}{L_i} \frac{\partial F^i}{\partial a_2} \frac{\partial F^i}{\partial a_2} \end{bmatrix},$$

$$V = \begin{bmatrix} \sum_{i=1}^{n} \frac{1}{L_i} \frac{\partial F^i}{\partial a_1} F_0^i \\ \sum_{i=1}^{n} \frac{1}{L_i} \frac{\partial F^i}{\partial a_2} F_0^i \end{bmatrix} \tag{A.10}$$

The standard deviations for the unknown parameters are:

$$\sigma_{a_k} = \left(\frac{S}{n-2} \right)^{1/2} (C_{kk}^{-1})^{1/2} \tag{A.11}$$

The classical algorithm [12] for determining a_1 and a_2 is the following:

1. collect the data measurements Y_i, X_1, X_2 and the standard deviations σ_{y_i}, $\sigma_{x_{j,i}}$;
2. make the initial guess for the unknown parameters a_1^0 and a_2^0;
3. using the initial guess for the unknown parameters and the measurements, calculate the conditional function (Eq. (A.7)) and its partial derivatives from Eq. (A.6);

4. calculate the weight factors (Eq. (A.8));
5. calculate the elements of matrix C and vector V (Eq. (A.10));
6. invert matrix C;
7. calculate vector A (Eq. (A.10)) and a_1 and a_2;
8. use newly calculated a_1 and a_2 as the initial guesses for step 2;
9. continue steps 2–8 until the change in a_1 and a_2 is less than a prescribed value;
10. calculate the standard deviations for a_1 and a_2 (Eq. (A.11));

References

[1] V. Gurau, M.J. Bluemle, E.S. De Castro, Y.M. Tsou, J.A. Mann, T.A. Zawodzinski, J. Power Sources 160 (2006) 1156–1162.
[2] A. Bejan, Convection Heat Transfer, John Wiley & Sons, 1984, p. 349.
[3] I. Cabasso, Y. Yuan, X. Xu, US 5,783,325, Gas Diffusion Electrodes Based on Poly (Vinylidene Fluoride Carbon Blends, Patent issued July 21, 1998.
[4] DuPont Fluoroproducts—Dispersions Properties and Processing Guide (Technical Information).
[5] M. Uchida, Y. Aoyama, N. Eda, A. Ohta, J. Electrochem. Soc. 142 (1995) 4143–4149.
[6] D. Bevers, R. Rogers, M. von Bradke, J. Power Sources 63 (1996) 193–201.
[7] G.G. Park, Y.J. Sohn, T.H. Yang, Y.G. Yoon, W.Y. Lee, C.S. Kim, J. Power Sources 131 (2004) 182–187.
[8] M. Mathias, J. Roth, J. Fleming, W. Lehnert, in: W. Vielstich, A. Lamm, H.A. Gasteiger (Eds.), Handbook of Fuel Cells Fundamentals, Technology and Applications, vol. 3, John Wiley & Sons Ltd., 2003, pp. 1–21.
[9] M.V. Williams, E. Begg, L. Bonville, H.R. Kunz, J.M. Fenton, J. Electrochem. Soc. 151 (2004) A1173–A1180.
[10] M. Bluemle, V. Gurau, J.A. Mann, T.A. Zawodzinski Jr., E.S. De Castro, Y.M. Tsou, 206 Meeting of the Electrochemical Society, Honolulu, HA, October 3–8, 2004.
[11] M. Bluemle, V. Gurau, J.A. Mann, T.A. Zawodzinski Jr., E.S. De Castro, Y.M. Tsou, 2004 Fuel Cell Seminar, San Antonio, TX, November 1–5, 2004.
[12] J.A. Mann Jr., in: E. Matijevic, R.J. Good (Eds.), Surface and Colloid Science, vol. 13, Plenum Press, New York, 1984, p. 213.